MEASUREMENT OF PHASE ACCUMULATION IN THE TRANSFER FUNCTIONS OF BEAMS AND PLATES

L. Wang and S. J. Walsh

Department of Aeronautical and Automotive Engineering

Loughborough University, Loughborough, LE11 3TU, U. K.

2 Copies Submitted

28 Manuscript pages

16 Figures

1 Table

RUNNING HEADLINE: Transfer Function Phase

ADDRESS FOR CORRESPONDENCE:

Dr S. J. Walsh

Department of Aeronautical and Automotive Engineering

Loughborough University

Loughborough, LE11 3TU. UK

ABSTRACT

Previous research into the phase of transfer functions from beam and plate-type structures has shown that the accumulated phase has different characteristics depending on whether the vibrational field is direct, diffuse, or between these two extremes. In this paper, these accumulated phase characteristics are numerically and experimentally investigated. Existing phase accumulation theories for direct and reverberant vibrational fields are presented. Predictions of the accumulated phase are then compared to measurements of the accumulated phase from the transfer mobilities of a number of beam and plate structures. It is shown that selection of the correct FFT frequency resolution in the experiment is vital in obtaining an accurate measurement of the phase of the transfer function. A criterion based upon the half-power bandwidth of the analysis frequency band is proposed as a basis to select the correct FFT frequency resolution. It is also shown that the location of the excitation may affect the measured value of the accumulated phase. Experimental results also show that the accumulated phase in a vibrational wave field between that of a direct field and a diffuse field is related to the source-receiver separation distance and to the damping in the structure. It is shown that the resulting accumulated phase curve lies between the direct field phase limit and the reverberant field phase limit.

1. INTRODUCTION

The transfer function between two points in a structure can be easily measured and is widely used to analyse the dynamic characteristics of a system. Often the phase of the transfer function is only inspected over a phase range from 0 to 2π radians. However, the accumulated or unwrapped phase of a transfer function may also reveal useful information about the structure since different types of wave fields will have different accumulated phase characteristics. For example, the phase accumulation in a diffuse field is much greater than the phase accumulation in a direct field. This phenomenon implies that the phase of a transfer function can be used to determine the level of diffusivity of a vibrational wave field. In this paper, the phase of a transfer function in both a direct field and a diffuse field will be investigated.

Research into the phase characteristics of transfer functions has received only limited attention in the past. One notable exception is Lyon and his co-investigators who have made a significant contribution in this area. In references [1,2], the relationship between phase accumulation and the poles and zeros of a transfer function was presented. Based upon this approach, it was shown that as the frequency increases the accumulated phase will increase by π radians if passing a zero and decrease by π radians if passing a pole. Further, for a finite, resonant, one-dimensional system the phase accumulation was shown to vary about the spatial or propagation phase, $-kr$. For a two-dimensional system the phase accumulation in a diffuse field was shown to vary about a trend line given by half the number of poles of the system multiplied by $\pi/2$ radians. An experimental

investigation of this ‘reverberant phase limit’ for steel and perspex plates was reported by Mondot and Petersson in reference [3]. Their measurements indicated that at high damping levels and high frequencies the measured transfer function phase deviated from the reverberant phase limit. In reference [4], the distribution of transfer function zeros in the complex frequency plane was studied by Tohyama and Lyon. They categorised the zeros into two different types: minimum phase zeros and non-minimum phase zeros. It was shown that non-minimum phase zeros have the same effect upon phase accumulation as poles. In reference [5], the effect of truncation of impulse response data on phase accumulation was studied. It was shown that the measured phase accumulation was sensitive to the window length of the truncated impulse response function. It was recommended that the exponential window should be used for the data processing in order to reduce the effect of truncation on the phase accumulations. In reference [6], the distribution of non-minimum phase zeros from transfer functions was studied and it was shown that the number of non-minimum phase zeros was inversely proportional to the damping in the system. The phase accumulation in a reverberant field was then predicted by using the group delay, which is the first derivative of the phase over frequency, $d\phi/d\omega$. The phase accumulation from this model is related to both the modal density and the damping of the system. Therefore, it is a function of the modal overlap of the system. This result then was employed for the pulse waveform recovery in a reverberant condition [7]. The phase variability in a reverberant field with high modal overlap was reported in reference [8] where it was shown that variability of the phase from its predicted trend was

due to the random occurrence of poles and zeros. This phase variability was studied in terms of the group delay. It was shown that the variance of the group delay was independent of frequency band and that it decreases as the damping in the system increases. The group delay for a lightly damped structural system excited by sound impingement was discussed in reference [9]. It was shown that in this case the group delay is roughly twice that of the point force excitation case. In reference [10], Fletcher and Thwaites investigated the conditions under which direct field propagation phase occurs in a reverberant environment based upon the poles and zeros approach through the study of phase accumulations characteristics. It was shown that propagation phase can be observed in a reverberant system provided the modal damping coefficient is very much greater than a ratio formed between the propagant distance and the size of the structure under test. In reference [10] Fletcher and Thwaites use the term ‘propagant phase’ in referring to the spatial or propagation phase. For the remainder of this paper the term propagant phase is also employed.

In this paper, phase accumulation characteristics in the transfer functions of beams and plates are investigated. In section two, the existing phase accumulation theories presented in references [1-10] are summarised. In section three, computer simulation results of the phase accumulation in the transfer functions of beams and plates supporting purely direct or purely diffuse vibrational fields are presented. In section four, experimental measurements of the accumulated phase are compared to corresponding predictions of the direct field phase and reverberant field phase. The measured results

show the importance of the selection of correct FFT frequency resolutions for obtaining accurate phase accumulation results. A criterion based upon the half-power bandwidth of the analysis frequency bandwidth is suggested to select the FFT frequency resolution. Other potential factors affecting the measured accumulated phase such as degenerate modes of the structure and the location of the excitation are also discussed.

2. THEORY OF PHASE ACCUMULATION

The phase relationship, $\phi(\omega)$, between source and receiver locations for simple "infinite" wave propagation in a direct field is given by the propagant phase

$$\phi_p(\omega) = - kr, \tag{1}$$

where k is the wavenumber and r is the distance between source and receiver locations. This propagant phase relationship has been successfully used by Petersson and Mondot [11] to identify wave conversion between flexural and longitudinal waves in a beam framework structure and also by Pinnington and Brisco to identify bending wave speeds within a tyre [12].

However, Lyon noted in reference [1] that in many instances the measured phase accumulation greatly exceed the propagant phase given by equation (1). Lyon attributed this effect to reverberant wave behaviour of the structure. Hence, Lyon studied the polynomial modal expansion of a transfer function and found that, as the frequency, ω, increases, the accumulated phase will undergo a phase change of $+\pi$ if passing a zero and a phase change of $-\pi$ if passing a pole. Thus, if N_p poles and N_z zeros have been

passed up to a frequency ω, the phase accumulation in the transfer function of a reverberant environment, $\phi_r(\omega)$, will be approximately [1]

$$\phi_r(\omega) = -(N_p - N_z)\pi \pm \pi/2, \tag{2}$$

where the term $\pi/2$ arises from the possibility of a pole or zero near $\omega = 0$. It can be seen from equation (2) that the problem of estimating the phase accumulation, therefore, becomes a problem of estimating the number of poles and zeros that occur within the frequency interval of interest. Since the poles are the natural frequencies of the system, methods of mode count estimation [14] can be used to estimate the number of poles, N_p.

Lyon [1,2] proposed that the number of zeros, N_z, can be estimated by considering the modal expansion of the transfer function, $H(\omega)$, between the source location, x_s, and the response location, x_r. Thus,

$$H(\omega) = const \sum_m \frac{\psi_m(x_s)\psi_m(x_r)}{\omega^2 - \omega_m^2} \tag{3}$$

where $\Psi_m(x_s)$ and $\Psi_m(x_r)$ are the mode shape functions of the structure and m is the mode count. It is assumed that the mode shape functions are real. Lyon further assumed that the summation in equation (3) could be replaced by considering two adjacent resonances, m and $(m+1)$, plus a remainder term, R. Thus,

$$H(\omega) \approx const\left[\frac{A_m}{\omega - \bar{\omega} + \varepsilon} + \frac{A_{m+1}}{\omega - \bar{\omega} - \varepsilon}\right] + \mathrm{R} \tag{4}$$

where $\bar{\omega} = (\omega_m + \omega_{m+1})/2$, $\varepsilon = (\omega_{m+1} - \omega_m)/2$ and the residues are given by $A_m = \Psi_m(x_s)\,\Psi_m(x_r)/2\omega_m$ and $A_{m+1} = \Psi_{m+1}(x_s)\,\Psi_{m+1}(x_r)/2\omega_{m+1}$. Lyon suggests that if the residues A_m and A_{m+1} have the same sign, a zero will exist between the two adjacent poles. The

remainder term does not affect the existence of a zero between the poles, but does slightly affect its location on the complex plane. If the residues A_m and A_{m+1} have different signs, there will not be a zero between the two adjacent poles.

Based upon the analysis of poles and zeros in the complex frequency plane, Lyon [1,2] found that the phase accumulation in a transfer function for a finite one-dimensional system follows the trend of the propagant phase, *-kr*. However, for a resonant, finite two-dimensional system, the phase accumulation greatly exceeds the propagant phase. In references [1,2] Lyon assumed that for a finite two-dimensional system the number of zeros, N_z, will be approximately half the number of poles, N_p. Thus, from equation (2) the phase accumulation will be

$$\phi_r(\omega) = -N_p \pi / 2 \qquad (5)$$

where for clarity of notation the additive term, $\pm\pi / 2$, has been omitted. In reference [2] Lyon termed $\phi_r(\omega)$ the reverberant phase limit and noted that the phase of a transfer function of a real two-dimensional structure will typically lie between the propagant phase curve given by equation (1) and the reverberant phase limit given by equation (5).

In reference [4] Tohyama and Lyon investigated the relationship between phase accumulation and the occurrence of double-zeros in the transfer function, $H(\omega)$. Double-zeros are either both located on the pole line or occur as a pair of complex conjugate zeros located symmetrically with respect to each other at equal distances from the pole line. If a conjugate zero is located below the real frequency axis, it is called a non-minimum phase zero. It was shown in reference [4] that a non-minimum phase zero

has the same effect upon phase accumulation as that of a pole. Thus, the accumulated phase will undergo a phase change of $-\pi$ if passing a non-minimum phase zero rather than a phase change of $+\pi$ as in the case for other types of zeros.

In references [6, 7] and [8] Tohyama, Lyon and Koike proposed that the accumulated phase, $\phi_r(\omega)$, was due to the number of "un-cancelled" poles plus the number of non-minimum phase zeros, N_z^+, in the transfer function, $H(\omega)$. Since the number of "un-cancelled" poles was equal to the number of non-minimum phase zeros and each non-minimum phase zero induces a phase change of $-\pi$ radians the accumulated phase can be expressed as

$$\phi_r(\omega) = -2\pi N_z^+ . \tag{6}$$

An example given in reference [6] showed the relationship of equation (6) to equation (5). In the example a reverberant field was considered. Therefore, it was deduced that the number of non-minimum phase zeros, N_z^+, was one quarter of the number of poles, N_p. Substituting this quantity into equation (6) led to equation (5). However, it was noted in reference [6] that equation (5) represented the total possible reverberant phase. As damping in the system increased the number of non-minimum phase zeros decreased. Hence, the reverberant phase limit, $\phi_r(\omega)$, also decreased. Because of phase variabilities due to the random occurrence of poles and zeros in the transfer function, $H(\omega)$, the reverberant phase limit, $\phi_r(\omega)$, was also evaluated in terms of the group delay

$$\tau_g(\omega) = \frac{d\phi_r}{d\omega} \tag{7}$$

which is the first derivative of the reverberant phase with respect to frequency. It was

shown in reference [6] that the group delay is given by

$$\tau_g(\omega) = -\frac{\pi}{2} n(\omega)[1 - \frac{2}{\pi}\tan^{-1}(\frac{2}{\pi}M)] \quad (8)$$

where $\tan^{-1}$ is the arctan function, $n(\omega)$ is the modal density of the system and $M(\omega)$ is the modal overlap defined by

$$M(\omega) = \frac{\pi}{2}\omega\eta n(\omega) \quad (9)$$

and η is the damping loss factor. Thus, the modal overlap, $M(\omega)$, is defined here in terms of energy bandwidth, which is equal the half-power bandwidth multiplied by $\pi/2$. Equations (8) and (9) indicate that as the damping loss factor, η, increases the reverberant phase limit, $\phi_r(\omega)$, decreases. Thus, because of the existence of damping in the system, equations (6), (7) and (8) should give a more accurate estimation of the reverberant phase limit, $\phi_r(\omega)$, than equation (5).

In the following sections, where the equations are not stated explicitly, then equation (1) is referred to as "the propagant phase", $\phi_p(\omega)$. The reverberant phase, $\phi_r(\omega)$, expressed by equation (2) is referred to as "the accumulated phase". The reverberant phase, $\phi_r(\omega)$, expressed by equation (5) is referred to as "Lyon's reverberant phase limit" and the reverberant phase, $\phi_r(\omega)$, expressed by equations (7) and (8) is referred to as "Tohyama's reverberant phase limit".

3. COMPUTER SIMULATION STUDY

To compare the phase accumulation in the transfer functions of a finite structure with

the propagant phase, *-kr*, of an equivalent "infinite" structure, computer simulations were undertaken for a straight beam and for a flat plate undergoing flexural vibrations.

3.1 A ONE-DIMENSIONAL WAVE FIELD: THE STRAIGHT BEAM

The simulated beam's dimensions and material properties are listed in Table 1 and were chosen to be the same as the experimental straight beam described in section 4. Equation (2) is employed to calculate the phase accumulation. The number of poles, N_p, can be theoretically obtained for the beam using the following equation [13], which assumes the beam is simply supported at both ends:

$$\omega_n = \sqrt{\frac{EI}{\rho A}} \cdot \frac{(n\pi)^2}{l^2} \qquad (10)$$

where E is Young's modulus, I is the second moment of area of the beam, ρ is the density, A the cross sectional area and l the length of the beam. The number of poles, N_p, is obtained by counting the number of natural frequencies, ω_n, below a given frequency, ω.

The number of zeros, N_z, is obtained using the pole-zero transfer function model, equation (4). The product of the mode shape functions for m^{th} mode of a simply supported beam is given by reference [13] as

$$\psi_m(x_s) \cdot \psi_m(x_r) = \sin(m\pi x_s / l)\sin(m\pi x_r / l) \qquad (11)$$

where x_s and x_r are the source and receiver positions, respectively. The number of zeros, N_z, up to a given frequency, ω, is developed by substituting equation (11) into equation (4) and considering the signs of the numerators of the two adjacent pole terms, A_m and A_{m+1}. If the signs of numerators for the successive pole terms are the same, there will be a zero

between those two poles and the number of zeros increases by one. Otherwise, it is assumed that there are no zeros between the interval of these two poles. It is also assumed that the force is applied at a position 0.2 m from one end and that the distance from the source to the receiver location is *r*. Thus, $x_s = 0.2$ m and $x_r = (0.2 + r)$ m.

Figure 1 shows the numerical results of the phase accumulation in the transfer function of the beam at different distances of *r* = 0.65 m, *r* = 0.9 m and *r* =1.1 m over the frequency range 0 to 3400 Hz. The solid lines in Figure 1 show the phase accumulation results calculated by using equation (2) and the dotted lines show the propagant phase, -*kr*, of an equivalent "infinite" beam. It can be seen in Figure 1 that the phase accumulations predicted using equation (2) for a finite beam undergo step changes of π or multiples of π radians. This is because of the phase change due to the poles and zeros of the transfer function. However, for each separation distance, *r*, the accumulated phase in the transfer function of the finite beam follows the trend of corresponding propagant phase, -*kr*, of the equivalent "infinite" structure.

3.2 A TWO-DIMENSIONAL WAVE FIELD: THE FLAT PLATE

To investigate the validity of Lyon's reverberant phase limit, $\phi(\omega) = -N_p \pi / 2$, for a flat plate, predictions of the accumulated phase were made using the pole-zero transfer function model, equation (4), and compared to calculations of the reverberant phase limit, $\phi(\omega) = -N_p \pi / 2$, for a flat plate. The simulated plate's dimensions and material properties were chosen to be the same as the experimental rectangular steel plate listed in

Table 1. The number of poles, N_p, is theoretically obtained for the plate by assuming a simply supported boundary condition [14]. Thus,

$$N_p(\omega) = \frac{\omega A}{4\pi\kappa c_l} \tag{12}$$

where c_l is the longitudinal wave speed in the material and κ is the radius of gyration of the cross-section of the plate. The reverberant phase limit, $\phi_r(\omega) = -N_p\pi/2$ is calculated using the number of poles, N_p, estimated from equation (12).

Equation (2) is employed to calculate the accumulated phase, $\phi(\omega)$. The number of zeros, N_z, is counted using the same method as that described for the simulated beam in section 3.1. Thus, the appropriate mode shape function is substituted in the pole-zero transfer function model, equation (4), and the sign of two adjacent pole terms considered to determine whether a zero exists. If so, the zero count, N_z, is increased by one. For a simply-supported plate, the mode shape function is given by reference [14] as

$$\psi_{m_1,m_2}(X_s)\cdot\psi_{m_1,m_2}(X_r) = \sin(m_1\pi x_s/l)\sin(m_2\pi y_s/w)\sin(m_1\pi x_r/l)\sin(m_2\pi y_r/w) \tag{13}$$

The plate is assumed to be excited at coordinate location $X_s(x_s,y_s)$ = (0.03 m, 0.07 m), and the response, $X_r(x_r,y_r)$, is assumed to be located at a distance r from the source.

Figure 2 shows predicted results for the phase accumulation, $\phi(\omega)$, against frequency in the transfer functions predicted at three different response locations: response location 1 with coordinates $X_r(x_r,y_r)$ = (0.18 m, 0.32 m), thus, the source-receiver separation distance, r, is 0.310 m; response location 2 with coordinates $X_r(x_r,y_r)$ = (0.16 m, 0.2 m), thus, the source-receiver separation distance, r, is 0.184 m; and response location 3 with coordinates $X_r(x_r,y_r)$ = (0.48 m, 0.27 m), thus, the source-receiver separation distance, r,

is 0.492 m. The thin solid lines show the accumulated phase, $\phi_{\square}(\omega)$, calculated using equation (2) for the three different separation distances, *r*. A prediction of the reverberant phase limit, $\phi_r(\omega) = -N_p\pi/2$, is shown as a thick solid line. Predictions of the propagant phase, *-kr*, for the three different separation distances, *r*, are shown with dashed lines. It can be seen in Figure 2 that the accumulated phase curves, $\phi_{\square}(\omega)$, calculated using equation (2), fluctuate with frequency because of the change of phase due to poles and zeros in the respective transfer functions, $H(\omega)$. However, all three curves follow the trend of the reverberant phase limit, $\phi_r(\omega) = -N_p\pi/2$. Since the reverberant phase limit, $\phi_r(\omega) = -N_p\pi/2$ is calculated from the number of poles of the plate, it will be independent of the source-receiver separation distance, *r*. It can also be seen in Figure 2 that all three accumulated phase curves, $\phi_{\square}(\omega)$, calculated for the finite plate are significantly greater than the corresponding propagant phase curves, *-kr*, of the equivalent "infinite" plate.

To illustrate the effect of damping, predictions of the reverberant phase limit for the rectangular steel plate were also made using Tohyama's reverberant phase model, equation (8). The damping of the structure, η, is assumed constant over the frequency range of interest, 0-3200 Hz. Three different damping conditions are assumed, with loss factors, η, of $4*10^{-4}$, $4*10^{-3}$ and 0.01. The source-receiver separation distance, *r*, was assumed to be 8.5 cm. To estimate the reverberant phase limit, the group delay, $\tau_g(\omega)$, was calculated using equation (8) and integrated with respect to frequency, ω, as shown in equation (7) to give the reverberant phase limit, $\phi_r(\omega)$. The modal density of the plate,

$n(\omega)$, was calculated by differentiating with respect to frequency the number of poles, N_p, given by equation (12). Thus,

$$n(\omega) = \frac{A}{4\pi\kappa c_l} \tag{14}$$

Figure 3 shows the phase accumulations against frequency predicted using Tohyama's reverberant phase model, equation (8), for the three different damping conditions. The reverberant phase limit, $\phi_r(\omega) = -N_p\pi/2$, and the progagant phase, -*kr*, are also shown. It can be seen in Figure 3 that as the damping in the plate increases, predictions of the phase from Tohyama's reverberant phase model accumulate less than that predicted by the reverberant phase limit, $\phi_r(\omega) = -N_p\pi/2$. When the damping is light, for example when η is $4*10^{-4}$, the phase accumulations from both models are similar. As the damping increases, for example when η is $4*10^{-3}$, the phase accumulation predicted using Tohyama's reverberant phase model is less than the reverberant phase limit, $\phi_r(\omega) = -N_p\pi/2$. When the damping is considerable, for example when η is 0.01, the phase accumulation predicted using the Toyama's model is considerably less than the reverberant phase limit, $\phi_r(\omega) = -N_p\pi/2$. It was noted by Tohyama, Lyon and Koike in reference [6] that this can be explained in terms of non-minimum phase zeros in the transfer function of the structure. Since, as the damping increases the number of non-minimum phase zeros, N_z^+, decreases and, hence, the phase accumulation, $\phi_{\square}(\omega)$, will be become less.

4. EXPERIMENTAL STUDY

4.1 A ONE-DIMENSIONAL WAVE FIELD: THE STRAIGHT BEAM

In the computer simulation presented in section three, it was shown that the phase accumulation in the transfer function of a straight beam undergoing flexural vibrations follows the trend of the propagant phase, $-kr$. To verify this prediction, the phase accumulation in the transfer functions of an experimental free-free steel beam was measured using the apparatus shown schematically in Figure 4. The rectangular steel beam was suspended by elastic ropes from a rigid frame and the beam was excited using random excitation from an electro-dynamic exciter located at one end of the beam. The applied force was measured with a force transducer at the excitation location and the response was measured with an accelerometer which was moved to different locations along the beam. The data acquisition and processing was carried out using an FFT analyzer, which calculated the required transfer functions. The material properties and physical dimensions of the beam are given in Table 1. The damping loss factor of the beam, η, was measured using the decay rate method [15] for the frequency range 15 Hz to 3215 Hz. Of course, transfer function phase can only be determined within a phase range from 0 to 2π radians. However, the measured transfer function phases were converted to continuous functions of frequency using the MATLAB ‘unwrap’ command. When using this command, if an absolute phase jump of greater than π radians is encountered then the phase value is changed to its 2π complement [16]. Ideally, a further check to ensure that the derivative is the same before and after the discontinuity should

also be performed. However, this is not implemented within the ‘unwrap’ command and was not performed for this analysis. Thus, using the ‘unwrap’ command an accumulated phase function was formed corresponding to each of the measured transfer functions.

Figure 5 shows the phase accumulation against frequency in the transfer functions of the beam measured at source-receiver separation distances, *r*, of 65 cm and 110 cm. The measurement frequency range was from 15 Hz to 3215 Hz. The solid lines shown in Figure 5 display the measured phase accumulations and the dotted lines show the corresponding theoretical predictions of the propagant phase, *-kr*. It can be seen in Figure 5 that the measured phase curves fluctuate in steps of π radians because of the phase change due to the resonances and anti-resonances of the structure. It can also be seen in Figure 5 that the measured phase accumulations follow the trends of the corresponding propagant phases, *-kr*. However, it is apparent in Figure 5 that the measured phase accumulation may deviate from the propagant phase curve, *-kr*, for significant frequency ranges. This occurs over the frequency range 1300 Hz to 2400 Hz for the accumulated phase measured at the source-receiver separation distance, *r*, of 65 cm. This discrepancy is due to the difference between the resonant and anti-resonant nature of the measured transfer function compared to the smooth behaviour of the propagant phase, *-kr*, of the equivalent infinite structure. For example, an anti-resonance at approximately 1300 Hz in the measured transfer function has induced a phase change of $+\pi$ radians in the measured phase moving it away from the propagant phase trend, *-kr*. This phase difference continues until a resonance is encountered at approximately 1800 Hz which induces a

phase change of $-\pi$ radians. Two further resonances at approximately 2250 Hz and 2400 Hz each induce a phase change of $-\pi$ radians moving the measured phase accumulation closer to the trend predicted by the propagant phase, *-kr*. At low frequencies, below approximately 80 Hz, the measured phase accumulations are corrupted by noise due to transducer limitations and, hence, the phase has not been accurately recorded.

4.2 A TWO-DIMENSIONAL WAVE FIELD: THE FLAT PLATE

In an ideal direct vibrational field, all of the waves travel away from the source. To obtain an experimental direct field, a perspex plate, with a relatively high damping loss factor, η, of $6*10^{-2}$, was supported in a wooden sandbox to create "infinite" wave propagation as illustrated schematically in Figure 6. The sandbox consisted of a square outer section of area 0.62 m by 0.62 m and a square inner section of area 0.28 m by 0.28 m. The perspex plate rested on a wooden inner section and sand was added both above and below the plate lying between the inner and outer sections of the box. The material properties and physical dimensions of the perspex plate are given in Table 1. For the sand to be an effective damping treatment, a minimum of at least one half of a wavelength of a bending wave should be within the sand. For this apparatus, 160 mm from the plate edge lay within the sand. Thus, "infinite" conditions are to be expected for bending waves above 210 Hz. An illustration of the effectiveness of the anechoic termination is shown in Figure 7 which displays on logarithmic axes the modulus of the point mobility of the perspex plate when excited by a force applied at its centre. The dotted horizontal line

shown in Figure 7 is the theoretical value of the modulus of the point mobility of the equivalent infinite plate [14]. As expected, the equivalent infinite mobility lies between the peaks and troughs of the measured point mobility. It can also be seen in Figure 7 that above approximately 300 Hz the peaks and troughs of the measured data lie close to the value of the equivalent infinite plate. Thus, indicating effective anechoic termination of the bending waves above this frequency.

A schematic representation of the measurement equipment is shown in Figure 8. The plate was excited by striking the centre location with an instrumented hammer which measured the applied force. The response was measured with a lightweight accelerometer at different locations on the plate. Data were collected and processed using an FFT analyser which calculated the necessary transfer functions.

Figure 9 shows the phase accumulation from three transfer mobilities of the plate measured over a frequency range of 0 Hz to 6400 Hz. The three lighter curves show the accumulated phase measured at the same distance of 14.1 cm but in three different directions. The theoretical value of the propagant phase, $-kr$, is shown as a bold line. It can be seen in Figure 9 that the measured data follow the trend of the propagant phase, $-kr$.

To verify the phase accumulation predictions for a diffuse vibrational field the transfer functions of two finite plates were measured using the experimental apparatus shown schematically in Figure 10. A square steel plate and a rectangular steel plate were suspended in turn using elastic ropes from a rigid frame giving free-free boundary conditions as illustrated in Figure 10. The material properties and physical dimensions of

the two test plates are given in Table 1. The damping loss factor of the two plates, η, was measured using the decay rate method [15]. Steel has relatively low structural damping compared to perspex and so waves reflected by the boundaries of the plates can be expected to generate a diffuse vibrational field. It is worth noting that there is also likely to be some loss of energy in the structure due to radiation damping. Each plate was excited using random excitation applied from an electro-dynamic exciter. The force was measured with a force transducer and applied at the centre of the plate or at an off-centre location. The response acceleration was measured with a lightweight accelerometer at a number of different distances from the source location. Frequency response function measurements were carried out using an FFT frequency analyser.

Figure 11 shows the measured phase accumulation in the transfer mobilities of the square plate plotted over a frequency range of 0Hz to 6400Hz. The excitation is applied at the centre of the plate and the response is measured at distances of 2, 4, 6, 8, 10, 12 and 14 cm from the exciter. For these measurements an FFT frequency resolution of 2 Hz/point was used. The direct field propagant phase, *-kr*, for a source-receiver separation distance of 2 cm is also shown. On this y-axis scale the propagant phase, *-kr*, appears to be the zero. However, when the scale is expanded, the propagant phase, *-kr*, is, as expected for the bending waves, proportional to the square root of frequency, $f^{1/2}$. The reverberant phase limit, $\phi_r(\omega) = -N_p \pi / 2$ is shown in Figure 11 as a straight line extending over the y-axis range from 0 to -250π radians. It can be seen in Figure 11 that all of the measured phase curves lie between the direct field propagant phase, *-kr*, and the reverberant phase limit,

$\phi_r(\omega) = -N_p\pi/2$. It can also be seen in Figure 11 that the gradient of the measured phase curves are approximately constant, but less than the slope of the reverberant phase limit, $\phi_r(\omega) = -N_p\pi/2$. It can also be seen that the measured phase accumulations lie close to one another except for the phase accumulation measured at the source-receiver separation distance, *r*, of 2 cm.

The fact that the experimental phase curves measured at source-receiver separation distances beyond 2 cm are all close to each other indicates that the accumulated phases have reached a certain limit with respect to the separation distance. However, this limit is much less that the reverberant phase limit, $\phi_r(\omega) = -N_p\pi/2$. This is not expected as the steel plate contains light damping, hence, the phase accumulation curves should lie close to the reverberant phase limit, $\phi_r(\omega) = -N_p\pi/2$. This characteristic of the accumulated phase is apparent in other studies on the accumulated phase in plates, for example in reference [10]. One explanation for the discrepancy, not noted in previous studies, is the fidelity of the FFT frequency resolution. Figure 12 shows the influence of different FFT frequency resolutions on the phase accumulation in three transfer functions measured on the steel plate. The excitation was applied at the centre of the plate and the response was measured at the same location 8.5 cm from the source. The three transfer functions were measured using FFT frequency resolutions of 0.5 Hz/Point, 1 Hz/Point and 2 Hz/Point. The accumulated phases of the three transfer functions are shown in Figure 12 along with the reverberant phase limit, $\phi_r(\omega) = -N_p\pi/2$, and the propagant phase, *-kr*. It can be seen in Figure 12 that as the FFT frequency resolution becomes finer the measured phase

accumulation increases towards the reverberant phase limit, $\phi(\omega) = -N_p \pi / 2$. This indicates that selection of the correct FFT frequency resolution is vital if accurate measurements of the accumulated phase are to be obtained.

To establish the required frequency resolution consider the case of a lightly damped structure whose frequency response function has been measured using a relatively coarse FFT frequency resolution. The two FFT phase values just before and just after a resonant frequency show a phase change of π radians. However, the phase tracking algorithm cannot detect whether this is a phase change of $+\pi$ radians and, hence, due to a zero or a phase change of $-\pi$ radians and, hence, due to a pole. What is required is an additional phase value between the phase jump of π radians that will establish the positive or negative direction of the phase change. Since the phase change of π radians can be expected to occur approximately over the half-power bandwidth, δf, of the resonance, three FFT data points will be required within the half-power bandwidth, δf. Thus, the proposed criterion for accurate measurement of the phase accumulation is that the FFT frequency resolution Δf, should be less than one half of the half-power bandwidth, δf. Hence,

$$\Delta f < \frac{1}{2} \delta f \ . \tag{15}$$

The half-power bandwidth, δf, can be expressed as [15]

$$\delta f = f \eta \tag{16}$$

where f is the resonant frequency of the mode. Thus, assuming the loss factor, η, is constant, it can be seen from equations (15) and (16) that a finer FFT frequency resolution, Δf, is needed at low frequencies, however, the resolution can be coarser at higher frequencies.

To illustrate the proposed FFT frequency resolution criterion, two transfer functions were measured both with FFT frequency resolutions better than the proposed resolution. For example, the rectangular steel plate with added damping treatment has a damping loss factor, η, measured using the decay rate method [15] for the frequency band from 50 Hz to 3250 Hz, of $2.1*10^{-2}$. Thus, above 200 Hz, an FFT frequency resolution of 1.05 Hz/Point is required to obtain accurate measurement of the accumulated phase. Figure 13 shows a comparison of the phase accumulation curves in the transfer function of the damped rectangular plate measured using FFT frequency resolutions of 0.25 Hz/Point and 1.0 Hz/Point respectively. Thus, both frequency resolutions are finer than the proposed maximum FFT frequency resolution of 1.05 Hz/Point. The source is located at a non-centre position and the two responses are measured at the same location, 8.5 cm from the source. It can be seen in Figure 13 that the measured phase accumulation curves are indistinguishable. This indicates that an FFT frequency resolution, Δf, of 1.0 Hz/Point is fine enough to ensure an accurate measurement of the accumulated phase in this case.

Another possible reason for the difference between the measured phase accumulation shown in Figure 12 and that predicted by the reverberant phase limit, $\phi(\omega) = -N_p \pi / 2$, is because of the existence of degenerate modes of the square plate. For a square or

rectangular plate there may be different mode shapes having the same natural frequency. This degeneracy is particularly pronounced for square plates [14]. When performing a phase accumulation the measured phase will change by π radians at each resonant frequency. However, if the resonance frequency corresponds to a degenerate mode then to correspond to the mode count of the reverberant phase limit, $\phi_r(\omega) = -N_p\pi/2$, the accumulated phase should change by a multiple of π radians. Since this is not the case, the measured accumulated phase will be an underestimate of the predicted accumulated phase.

A further reason for the difference between the measured phase accumulation shown in Figure 12 and that predicted by the reverberant phase limit, $\phi_r(\omega) = -N_p\pi/2$, is because the excitation was applied at the centre of the plate, and, hence, located on a nodal line. Thus, any mode shape with a nodal line at the centre of the plate will not be excited and, hence, will not be measured in the accumulated phase.

The effect of degeneracy and nodal line excitation upon the number of modes that can be counted in the amplitude spectra of a point excited rectangular plate has previously been illustrated in reference [14]. Hence, to minimise the effect of degenerate modes of the plate upon the phase accumulation the square plate was replaced by a rectangular steel plate. Further, to minimise the effect of exciting the plate on a nodal line the source was relocated from the centre of the plate to an off-centre position. To ensure a sufficiently fine FFT frequency resolution, a resolution of 0.25 Hz/point was used. The material properties and physical dimensions of the rectangular steel plate used for the experiment

are listed in Table 1.

Figure 14 shows the influence of different source locations upon measured phase accumulations. The two thin lines in Figure 14 show the measured phase accumulation for two transfer functions, one with the force applied at the centre of the plate and the other for the force applied at an off-centre location, but with the separation distance, *r*, between the source and the receiver remaining the same at 8.5 cm. The reverberant phase limit, $\phi(\omega) = -N_p \pi / 2$, and the propagant phase, *-kr*, are also shown. It can be seen in Figure 14 that phase accumulation corresponding to the off-centre excitation lies closer to the reverberant phase limit, $\phi(\omega) = -N_p \pi / 2$, than the phase accumulation in the transfer function measured with central excitation. This indicates that an off-center force excites more modes and, hence, produces greater phase accumulation. However, the effect of degeneracy is less clear. For example, the phase difference between the 0.5 Hz/Point phase accumulation curve and the reverberant phase limit, $\phi(\omega) = -N_p \pi / 2$, for the square plate data shown in Figure 12, is approximately 15π radians at 1600 Hz. This is approximately the same as the phase difference between the centre excitation phase accumulation curve and the reverberant phase limit, $\phi(\omega) = -N_p \pi / 2$, for the rectangular plate data at 1600 Hz shown in Figure 14. Thus, indicating that degeneracy may not be a significant phenomenon.

To illustrate the effect of source-receiver separation distance upon phase accumulation, phase accumulation curves were measured at four different separation distances, *r*, of 5.7 cm, 8.5 cm, 11.3 cm and 17.0 cm on the undamped rectangular steel plate. The source was

located at a non-centre position and the FFT frequency resolution of the data was 0.125 Hz/Point below 800 Hz and 0.25 Hz/Point above this frequency. It can be seen in Figure 15 that three of the measured accumulated phase curves lie close to the reverberant phase limit, $-\frac{\pi}{2}N_p$. The exception is the phase accumulation measured at the separation distance, *r*, of 5.7 cm, which suggests that the accumulated phase curves will reach the reverberant phase limit, $-\frac{\pi}{2}N_p$, at a source-receiver separation distance between 5.7 cm and 8.5 cm. It can also be seen in Figure 15 that the phase accumulation curves measured at 8.5 cm, 11.3 cm and 17.0 cm vary about Lyon's reverberant phase limit, $-\frac{\pi}{2}N_p$. One possible explanation for this variability is that only one transfer function measurement was made for each source-receiver separation distance, *r*. Therefore, the measured transfer function will be dependant upon the source location, as noted previously, and also upon the exact response location. In principle, a better estimate of the accumulated phase will be obtained by forming a spatial average from a number of transfer functions measurements made at the same source-receiver separation distance, *r*, but at different locations over the plate.

To study the effect of source-receiver separation distance upon phase accumulation characteristics under relatively high damping conditions, additive damping treatment was attached to one face of the rectangular steel plate. Due to the damping treatment, the plate loss factor increased significantly from $4.11*10^{-4}$ to $2.1*10^{-2}$ for the frequency analysis

band 50-3250 Hz. Measurements were made of the accumulated phase at separation distances, *r*, of 8.5, 17.0, 25.5, 34.0, 42.5 and 48.1 cm. The source was at a non-centre position and the FFT frequency resolution of the measured data was 1 Hz/point. Figure 16 shows the measured phase accumulation curves together with the reverberant phase limit, $-\frac{\pi}{2}N_p$, and the theoretical curve predicted using Tohyama's reverberant phase model, equation (8), which includes the effect of damping. The phase accumulation curves measured at source-receiver separation distances, *r*, of 42.5 cm and 48.1 cm lie close to the phase accumulation curve predicted by Tohyama's reverberant phase model, equation (8). It can be seen in Figure 16 that all of the measured phase accumulation curves are less than predicted by Lyon's reverberant phase limit, $-\frac{\pi}{2}N_p$. It can also been seen in Figure 16 that the phase accumulation curves for separation distances less than 42.5 cm are less than the accumulated phase predicted by Tohyama's reverberant phase model. However, as the source-receiver separation distance increases, the accumulated phase curves approach Tohyama's reverberant phase model. This indicates that Lyon's reverberant phase limit, $-\frac{\pi}{2}N_p$, is only suitable for light damped structures and that Tohyama's reverberant phase model is more appropriate when predicting the phase accumulation under relatively high damping conditions. Figure 16 also indicates that up to a certain source-receiver separation distance the phase accumulation is related to the separation distance and that beyond that critical distance the accumulated phase can be predicted

accurately using Tohyama's reverberant phase model, equation (8).

5. SUMMARY

For a finite one-dimensional structure, such as a beam, it has been shown that the transfer function phase, $\phi(\omega)$, fluctuates around the propagant phase, *-kr*. For a two-dimensional structure supporting a direct vibrational field such as an "infinite" plate it was shown that the measured transfer function phase also follows the trend predicted by propagant phase, *-kr*. By contrast, for a diffuse vibrational field, such as that in a lightly damped finite plate, the measured transfer function phase follows the reverberant phase limit, $-\frac{\pi}{2}N_p$, proposed by Lyon. It has also been shown that for a vibrational wave field containing both a direct field and a reverberant field, such as that in a heavily damped plate, the measured transfer function phase lies between the propagant phase, *-kr*, and Tohyama's reverberant phase limit given by equation (8). As the separation distance, *r*, between the source and the receiver locations increases, the measured transfer function phase also increases until it reaches Tohyama's reverberant phase limit. Beyond this separation distance, the measured transfer function phase will not show any increase with increasing separation distance.

This study has also illustrated two other factors which can affect the measured transfer function phase accumulation: (i) source location; and (ii) FFT frequency resolution. The source position has an influence on the measured phase accumulation in

that an off-centre source location will produce more phase accumulation than a central source location. This is because the excitation is now away from the central nodal lines and, hence, more modes are excited giving greater phase accumulation. Of particular importance in the accurate measurement of transfer function phase is the selection of the appropriate FFT frequency resolution. It has been shown that the FFT frequency resolution should be less than half of the half-power bandwidth of the analysis band Otherwise the positive or negative direction of a π radian phase jump due to a zero or a pole, respectively, may not be determined.

REFERENCES

1. R. H. LYON 1983 *Journal of the Acoustical Society of America* **73**(4), 1223-1228. Progressive phase trends in multi-degree-of freedom systems.
2. R. H. Lyon 1984 *Journal of the Acoustical Society of America* **76**(5), 1433-1437. Range and frequency dependence of transfer function phase.
3. J. M. MONDOT and B. PETERSSON 1986 *Proceedings of Inter-Noise 86*, 651-654. On the phase of transfer mobility functions.
4. M. TOHYAMA and R. H. LYON 1989 *Journal of the Acoustical Society of America* **86**(5), 1854-1863. Zeros of a transfer function in a multi-degree-of-freedom vibrating system.
5. M. TOHYAMA and R. H. LYON 1989 *Journal of the Acoustical Society of America* **86**(5), 2025-2029. Transfer function phase and truncated impulse response.

6. M. TOHYAMA, R. H. LYON and T. KOIKE 1991 *Journal of the Acoustical Society of America* **89**(4), 1701-1707. Reverberant phase in a room and zeros in the complex frequency plane.
7. M. TOHYAMA, R. H. LYON and T. KOIKE 1992 *Journal of the Acoustical Society of America* **91**(5), 2805-2812. Pulse waveform recovery in a reverberant condition.
8. M. TOHYAMA, R. H. LYON T. KOIKE 1994 *Journal of the Acoustical Society of America* **95**(1), 286-296. Phase variabilities and zeros in a reverberant transfer function.
9. H. HE and R. H. LYON 1996 *Journal of the Acoustical Society of America* **99**(3), 1465-1474. Group delay in resonant scattering.
10. N. H. FLETCHER and S. THWAITES 1996 *Journal of the Acoustical Society of America* 99(1), 314-323. Propagant phase in reverberant environments.
11. B. PETERSSON and J. M. MONDOT 1988 *Proceedings of Inter-Noise 88*, 455-460. The role of transfer mobilities in source characterisation.
12. R. J. PINNINGTON and A. R. BRISCO 2002 *Journal of Sound and Vibration* **253**(5), 941-959. A wave model for a pneumatic tyre belt.
13. S. S. RAO 1990 *Mechanical Vibrations*. Addison-Wesley, Reading, Massachusetts.
14. L. CREMER, M. HECKL AND E. UNGAR 1973 *Structure-Borne Sound.* 2nd Edition, Springer-Verlag, Berlin.
15. R. H. LYON and R. G. DEJONG 1995 *Theory and Application of Statistical Energy Analysis*. 2nd Edition, Butterworth-Heinemann.

16. MATLAB v 5.2.1, The MathsWorks Inc, Natick, Maryland, USA.

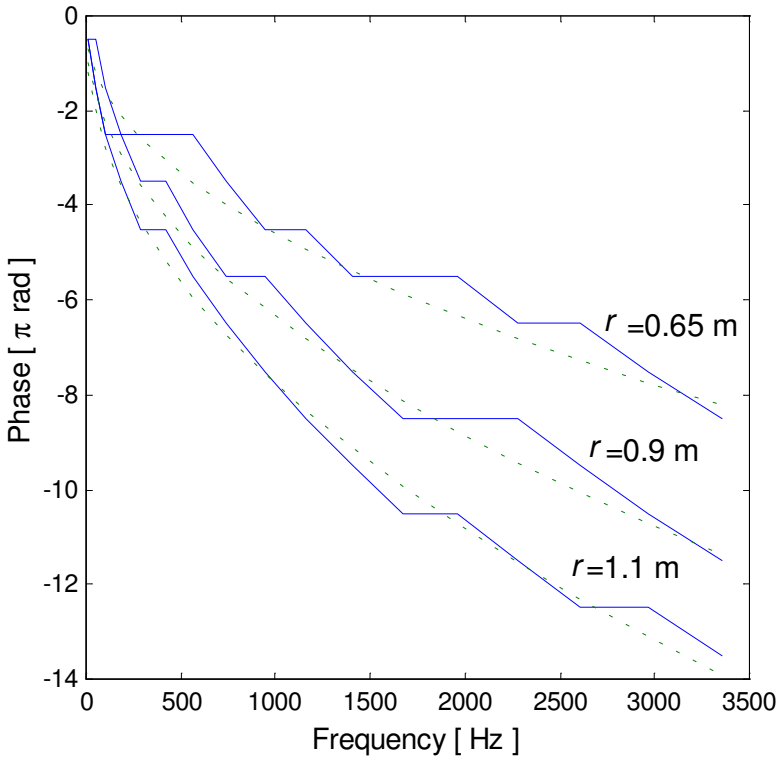

Figure 1. Phase accumulation against frequency in the transfer functions of a simple supported beam for three different source-receiver separation distances, r: ___, predicted using equation (2); ---, propagant phases, $-kr$, for the three separation distances, r.

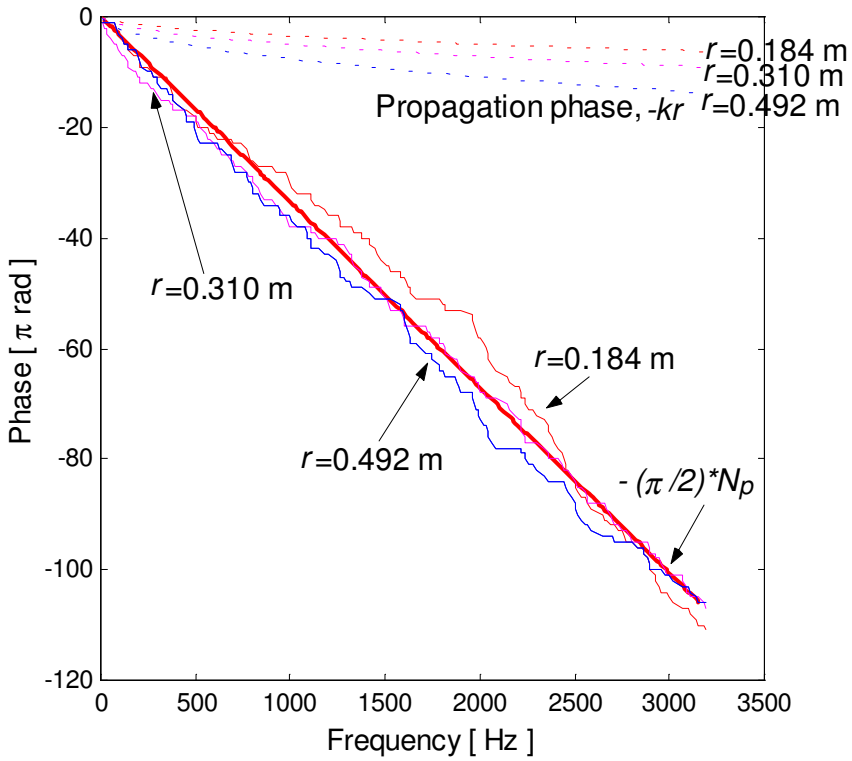

Figure 2. Phase accumulation against frequency in the transfer functions of a simply-supported steel plate: ___, predicted using equation (2) for three different source-receiver separation distances, r; ___, reverberant phase limit, $-(\pi/2)*N_p$; ---, propagant phases, $-kr$, for the three different separation distances, r.

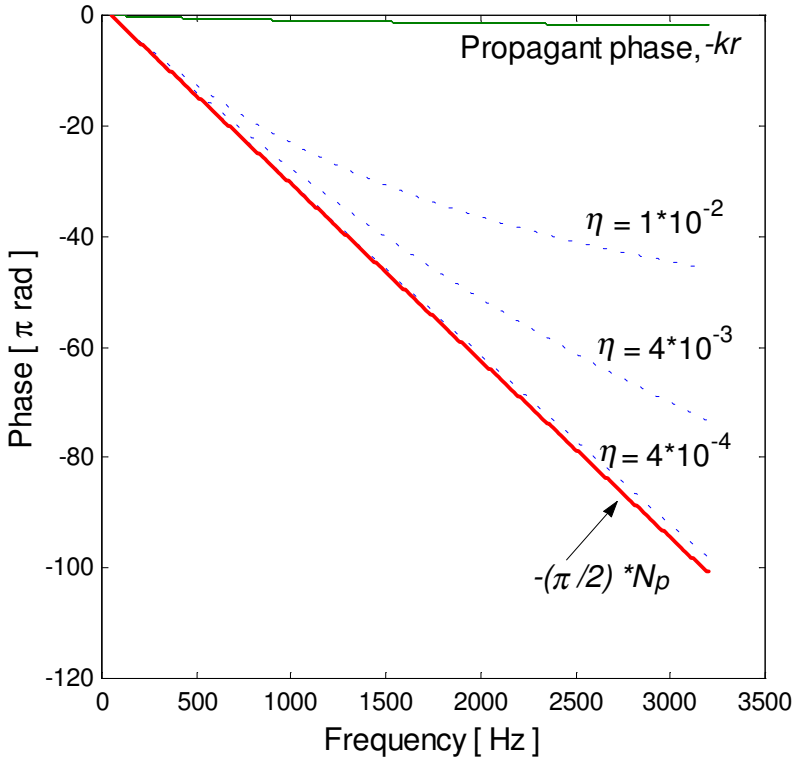

Figure 3. Phase accumulation against frequency in the transfer functions of a simply-supported steel plate with a source-receiver separation distance, *r*, of 8.5 cm: - --, predicted using Tohyama's reverberant phase model, equation (8), for three different damping conditions; ___, reverberant phase limit, $-(\pi/2)*N_p$; ___, propagant phase, $-kr$.

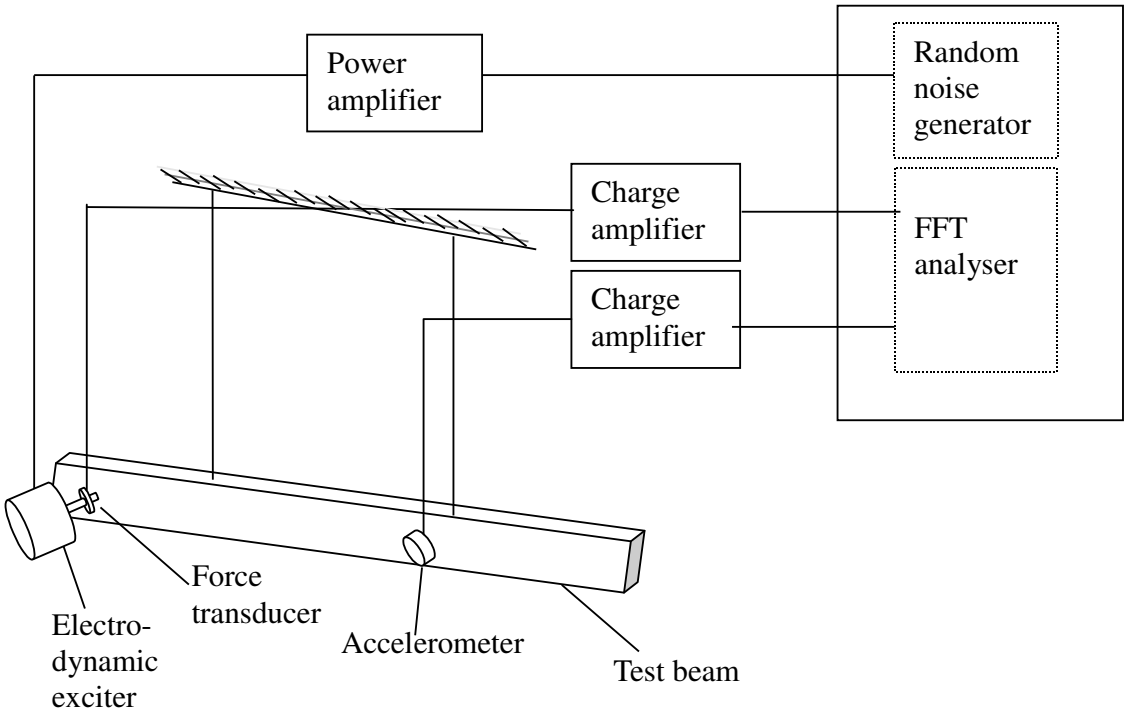

Figure 4. Apparatus used to measure the transfer functions of the experimental steel beam.

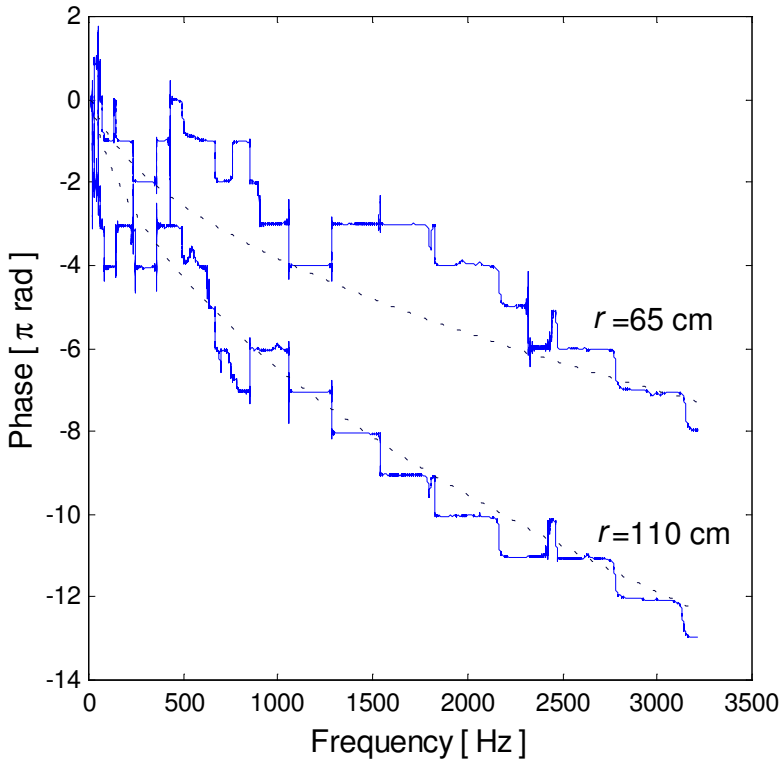

Figure 5. Comparison of experimental and theoretical phase accumulation in the transfer functions of the free-free beam for two different source-receiver separation distances, *r*: ___, measured phase accumulations; ---, propagant phases, *-kr*.

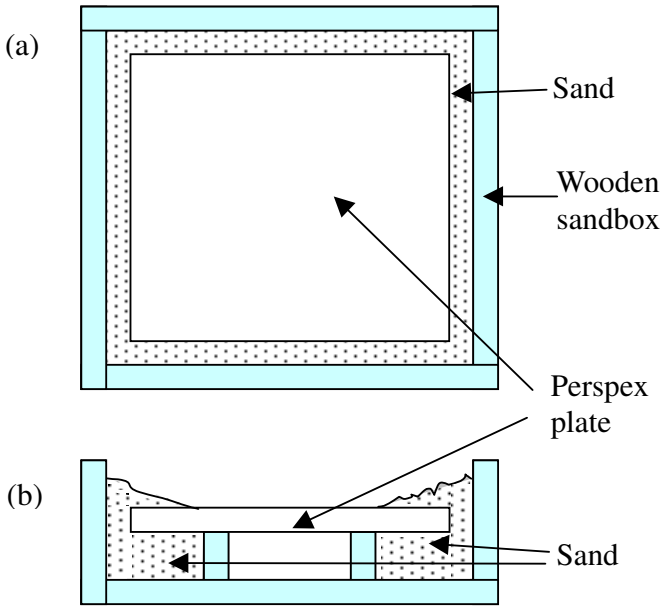

Figure 6. Laboratory apparatus used to create a direct vibrational field in the "infinite" perspex plate: (a) top view; (b) side view.

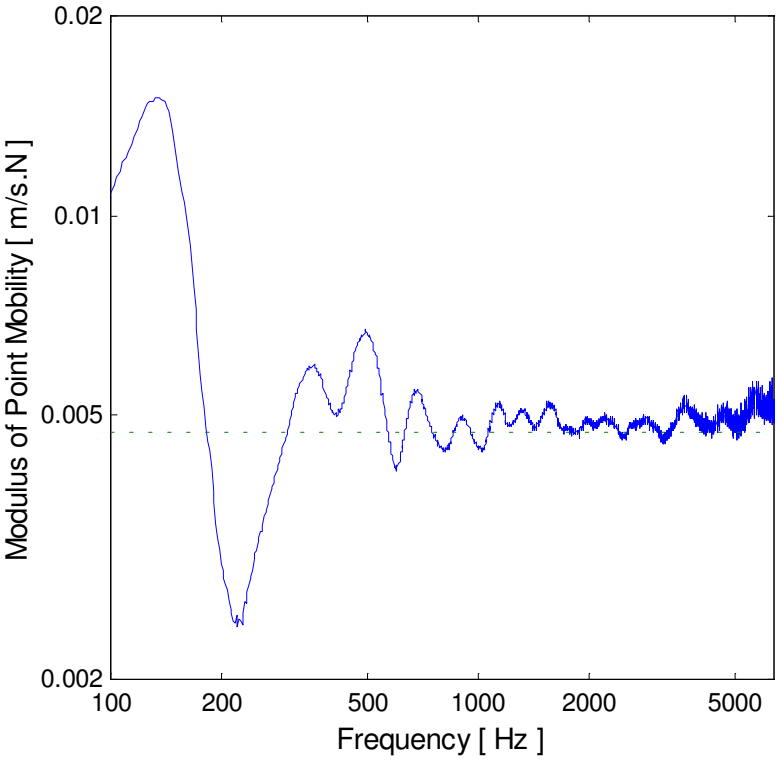

Figure 7. Modulus of the point mobility of the "infinite" perspex plate: ___, measured data; ---, theoretical value of the equivalent infinite structure.

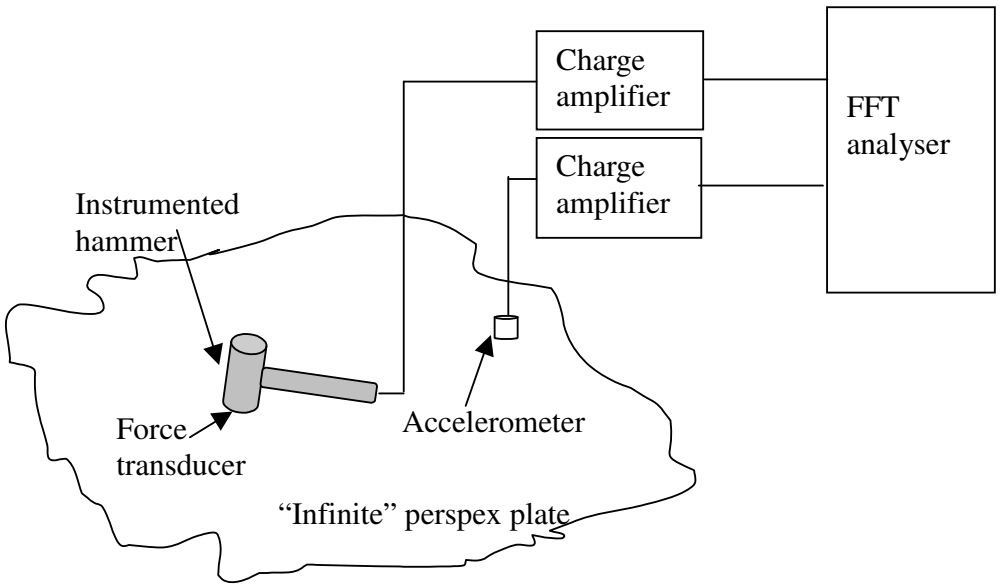

Figure 8. Equipment used to measure the transfer functions of the experimental “infinite” perspex plate.

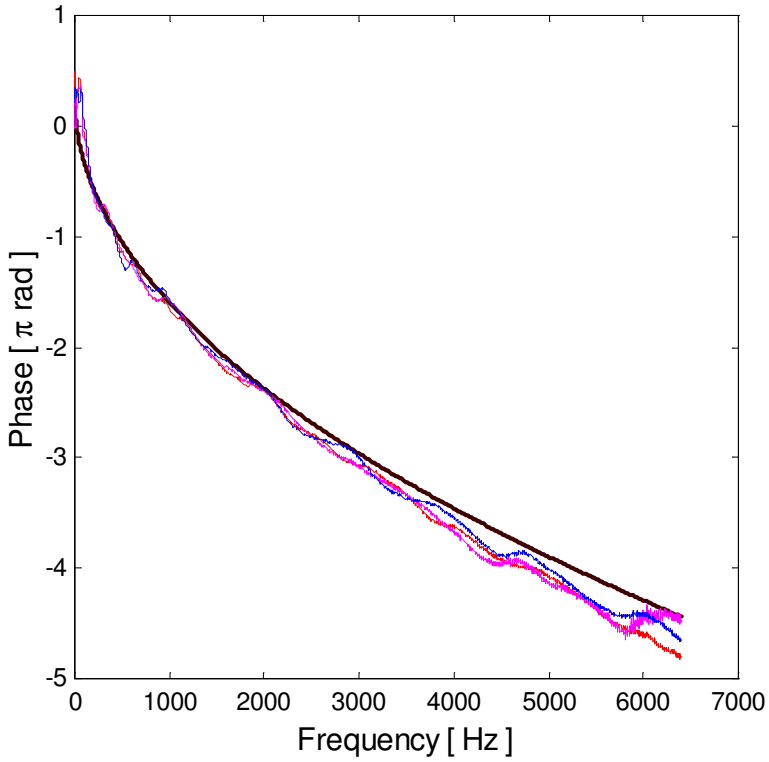

Figure 9. Comparison of experimental and theoretical phase accumulation in the transfer functions of the "infinite" perspex plate: ___, measured phase accumulations in three different directions for the same source-receiver separation distance, *r*, of 14.1 cm; ___, propagant phase, *-kr*.

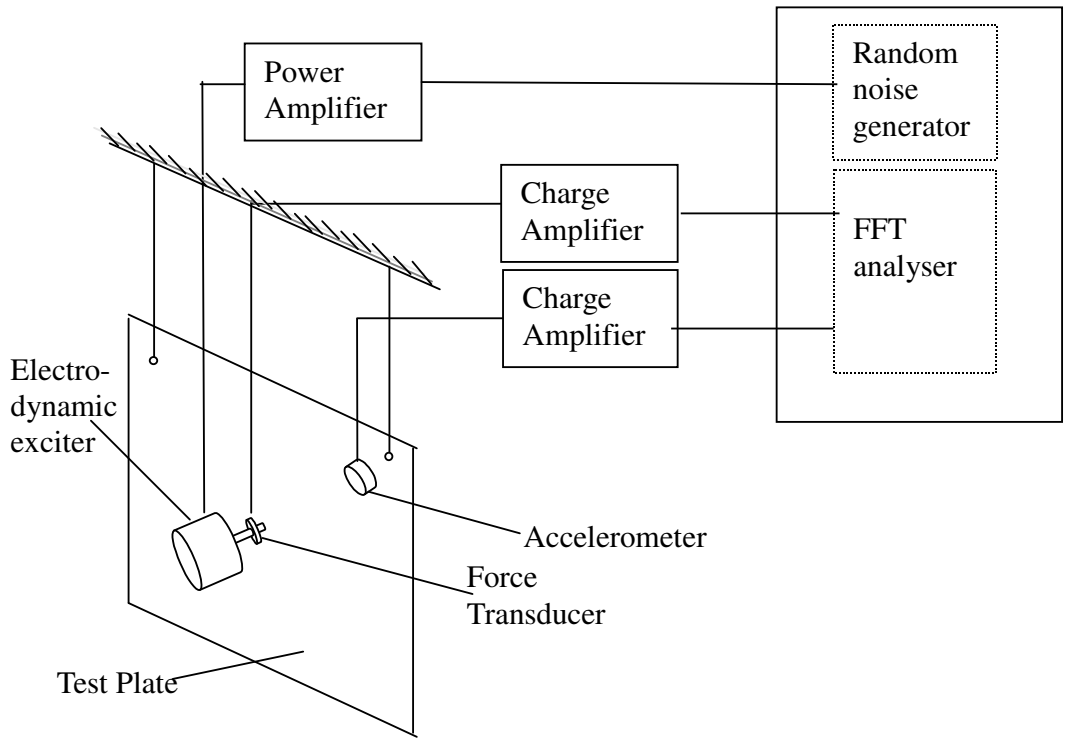

Figure 10. Apparatus used to measure the transfer functions of the experimental steel plates.

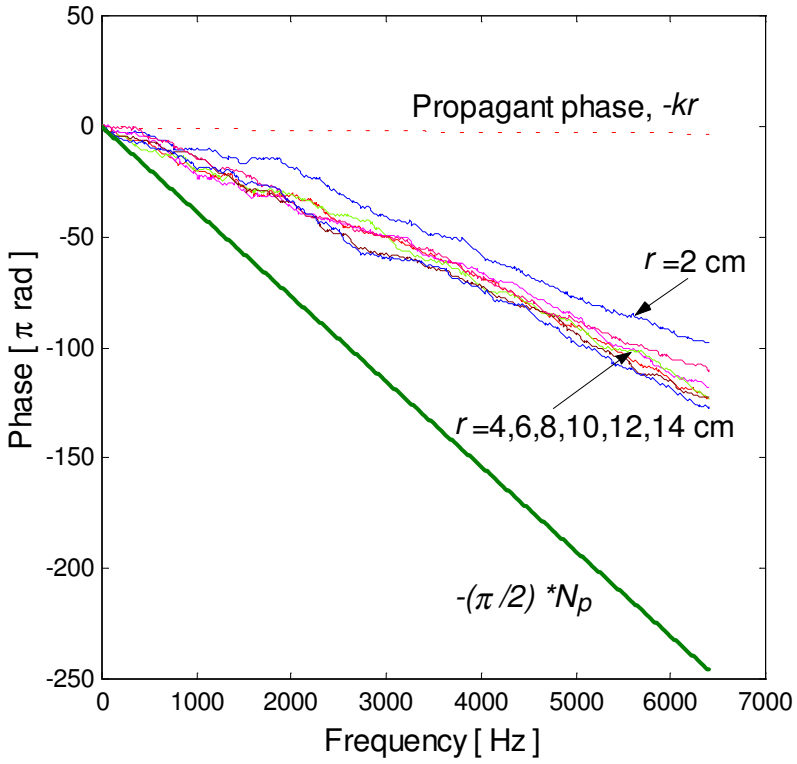

Figure 11. Comparison of experimental and theoretical phase accumulation in the transfer functions of the free-free square steel plate with the excitation applied at the centre: ___, measured phase accumulations for different source-receiver separation distances, *r*; ___, reverberant phase limit, $-(\pi/2)*N_p$; ---, propagant phase, $-kr$, for the source-receiver separation distance, *r*, of 2 cm.

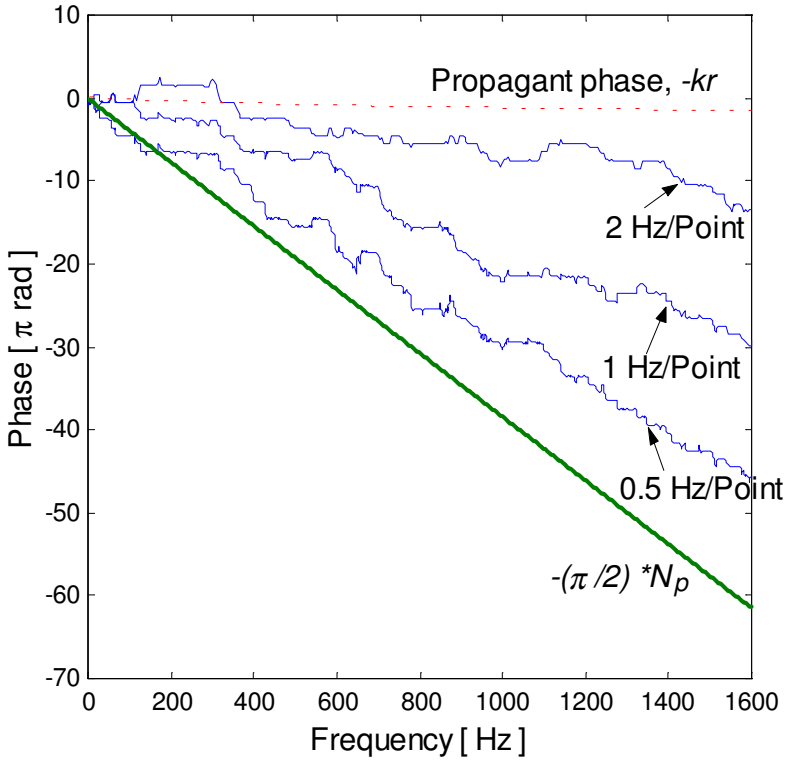

Figure 12. Influence of different FFT frequency resolutions on the measured phase accumulation in the transfer functions of the free-free square steel plate with the excitation applied at the centre and a source-receiver separation distance, *r*, of 8.5cm: ___, measured phase accumulations for three different FFT frequency resolutions; ___, reverberant phase limit, $-(\pi/2)*N_p$; ---, propagant phase, $-kr$.

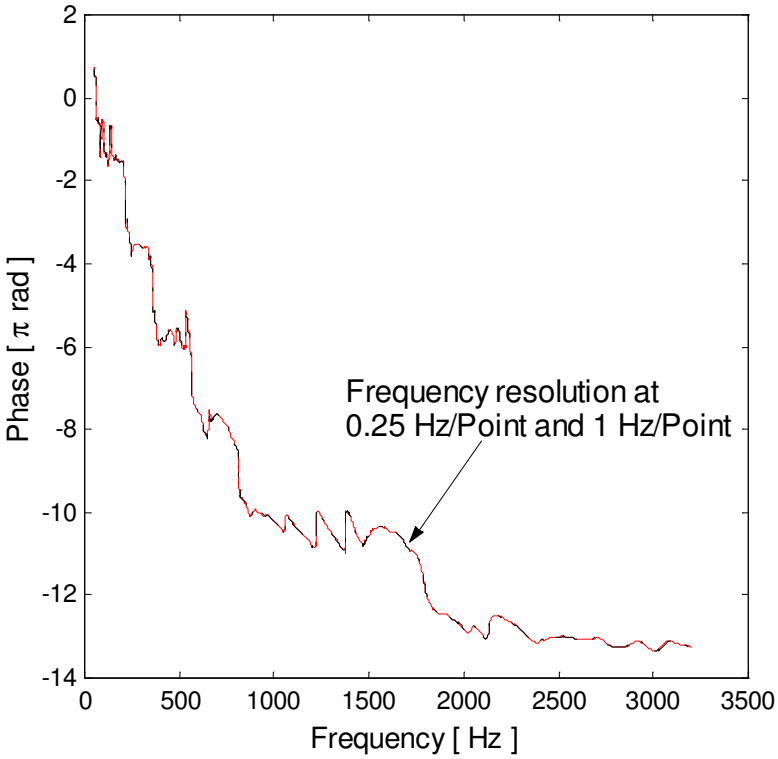

Figure 13. Influence of FFT frequency resolution on the measured phase accumulation in the transfer functions of the free-free rectangular steel plate with additive damping treatment (η=2.1*10^{-2}) with the excitation applied at a non-centre location and the response measured at a source-receiver separation distance, *r*, of 8.5 cm: ___, measured phase accumulations at 0.25 Hz/Point FFT frequency resolution and 1 Hz/Point FFT frequency resolution.

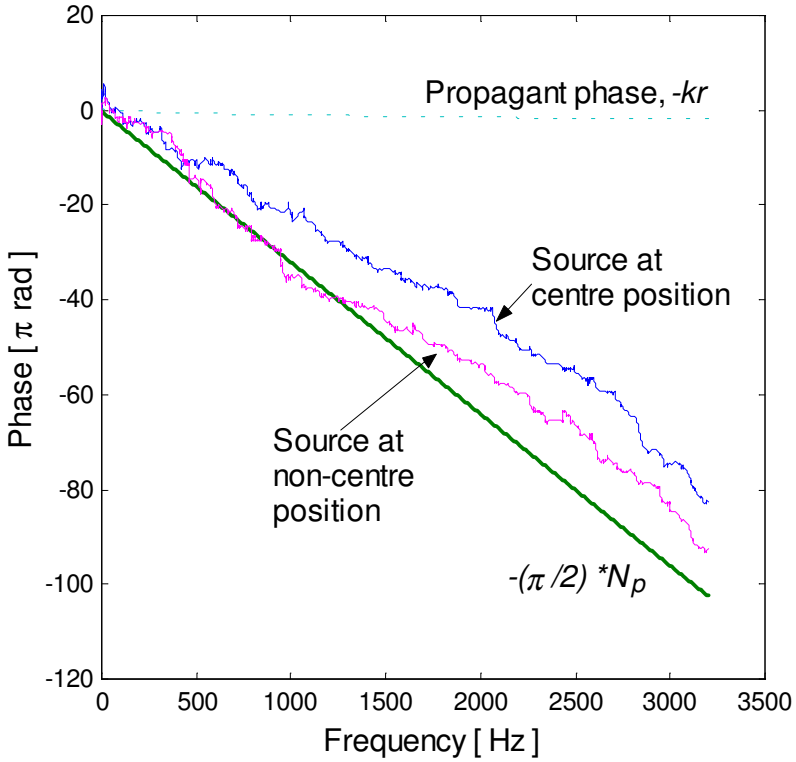

Figure 14. Influence of different excitation locations on the measured phase accumulation in the transfer functions of the free-free rectangular steel plate at a source-receiver separation distance, *r*, of 8.5 cm: ___, measured phase accumulations with the source applied at the centre and with the source applied at an off-centre location; ___, reverberant phase limit, $-(\pi/2)*N_p$; ---, propagant phase, $-kr$.

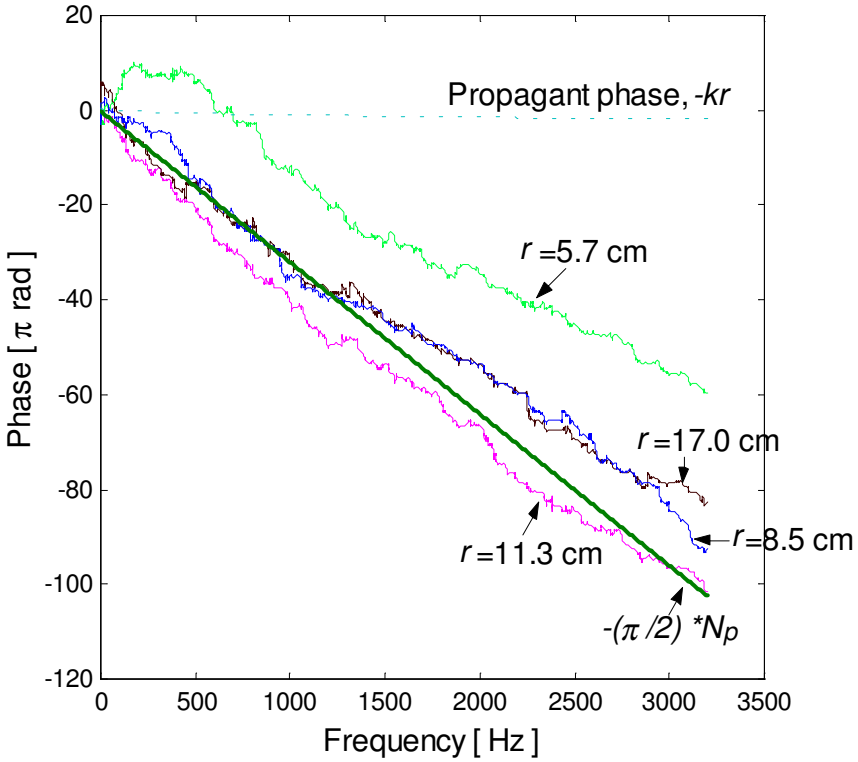

Figure 15. The effect of source-receiver separation distance in the phase accumulation of the transfer functions of the free-free rectangular steel plate with the excitation applied at a non-centre position: ___, measured phase accumulations for four different separation distances, *r*; ___, reverberant phase limit, $-(\pi/2)*N_p$; ---, propagant phase, *-kr*, for the distance, *r*, of 5.7 cm.

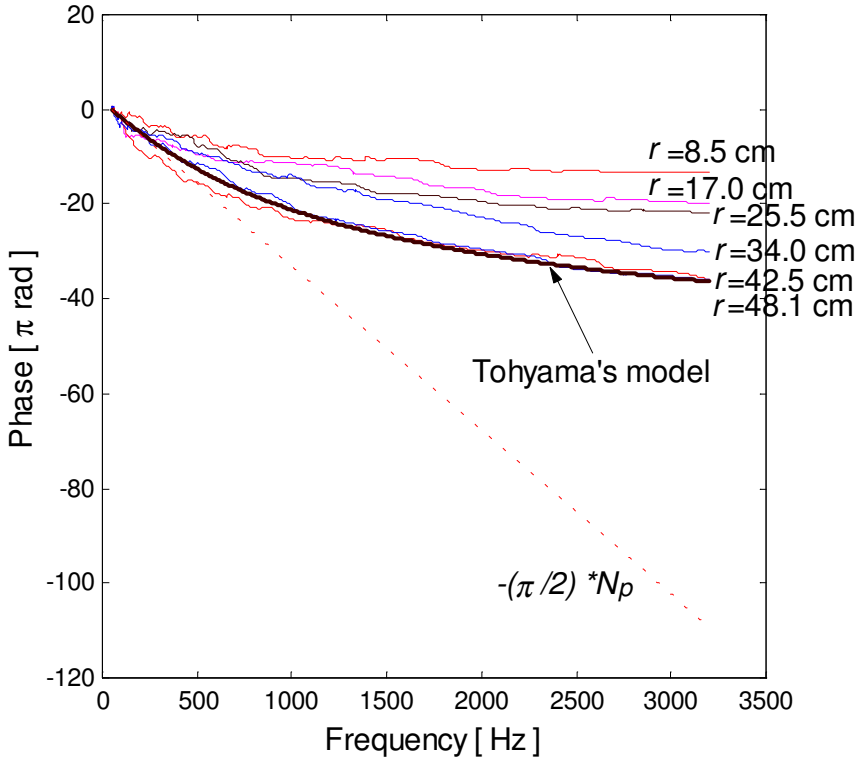

Figure 16. Comparison of Tohyama's diffuse field phase model, equation (8), with the measured phase accumulation in the transfer functions of the free-free rectangular steel plate with additive damping treatment (η=2.1*10^{-2}) with the excitation applied at a non-centre location: ___, measured phase accumulations for different separation distances, r; ___, Tohyama's reverberant phase model, equation (8); ---, reverberant phase limit, $-(\pi/2)*N_p$.

Structure	Young's modulus, E (N/m^2)	Density, ρ (kg/m^3)	Poisson's ratio, υ	Loss factor, η	Length, l (m)	Width, w (m)	Thickness, h (m)
Perspex Plate	$5.0*10^9$	1180	0.3	$6.0*10^{-2}$	0.6	0.6	0.006
Steel beam	$210*10^9$	7870	0.3	$5.0*10^{-4}$	1.385	0.019	0.0095
Square steel plate	$210*10^9$	7870	0.3	$1.84*10^{-4}$	0.6	0.6	0.0015
Rectangular steel plate	$210*10^9$	7870	0.3	$4.11*10^{-4}$	0.8	0.5	0.002
Rectangular steel plate with added damping	$210*10^9$	7870	0.3	$2.1*10^{-2}$	0.8	0.5	0.002

TABLE 1. *Dimensions and material properties of the experimental beam and the four experimental plates.*